Pulsed Laser Imaging of Rapid Ca^{2+} Gradients in Excitable Cells

Jonathan R. Monck,* Iain M. Robinson,* Ariel L. Escobar,‡ Julio L. Vergara,‡ and Julio M. Fernandez*
*Mayo Clinic, Department of Physiology and Biophysics, Rochester, Minnesota 55905, and ‡Department of Physiology, University of California at Los Angeles, Los Angeles, California 90024 USA

ABSTRACT Excitable cells are thought to respond to action potentials by forming short lived and highly localized Ca^{2+} gradients near sites of Ca^{2+} entry or near the site of Ca^{2+} release by intracellular stores. However, conventional imaging techniques lack the spatial and temporal resolution to capture these gradients. Here we demonstrate the use of pulsed-laser microscopy to measure Ca^{2+} gradients with submicron spatial resolution and millisecond time resolution in two preparations where the Ca^{2+} signal is thought to be fast and highly localized: adrenal chromaffin cells, where the entry of Ca^{2+} through voltage dependent Ca^{2+} channels triggers exocytotic fusion; and skeletal muscle fibers, where intracellular Ca^{2+} release from the sarcoplasmic reticulum initiates contraction. In chromaffin cells, Ca^{2+} gradients developed over 10–100 ms and were initially restricted to discrete submembrane domains, or hot spots, before developing into complete rings of elevated Ca^{2+} concentration. In frog skeletal muscle large, short-lived (~6 ms) Ca^{2+} gradients were observed within individual sarcomeres following induction of action potentials. The pulsed laser imaging approach permits, for the first time, the capture and critical examination of rapid Ca^{2+} signaling events such as those underlying excitation-secretion and excitation-contraction coupling.

INTRODUCTION

Ca^{2+} entry through Ca^{2+} channels during action potentials is the trigger for exocytosis in excitable secretory cells (Douglas, 1968). The observation that exocytosis is triggered more effectively by agents that stimulate Ca^{2+} influx than those that mobilize intracellular Ca^{2+}, and discrepancies between the Ca^{2+} sensitivity of exocytotic responses and measured, spatially averaged Ca^{2+} changes during depolarization of chromaffin cells led to the suggestion that spatially localized Ca^{2+} increases might be responsible for triggering exocytosis (Cheek et al., 1989; Augustine and Neher, 1992). Models of Ca^{2+} entry, Ca^{2+} binding, and diffusion have predicted that the opening of Ca^{2+} channels causes the formation of a ring-like Ca^{2+} gradient reaching a concentration of tens or hundreds of micromolar just beneath the plasmalemma (Sala and Hernandez-Cruz, 1990; Nowycky and Pinter, 1993). However, efforts to capture these Ca^{2+} signals in adrenal chromaffin cells using existing Ca^{2+} imaging techniques with a resolution in the hundreds of milliseconds have detected a much smaller (<1 μM) Ca^{2+} gradient around the cell periphery during prolonged (100 ms or longer) depolarizations (O'Sullivan et al., 1989; Cheek et al., 1989; Neher and Augustine, 1992). Limitations in imaging technology have prevented Ca^{2+} measurements at earlier times. Whether the measured Ca^{2+} gradients represent temporally low-passed filtered remnants of much larger (>100 μM) gradients occurring shortly after Ca^{2+} channel opening remains unknown. It is important to understand the nature of the Ca^{2+} signal for exocytosis because the magnitude of the Ca^{2+} gradient will help define the types of Ca^{2+} binding proteins that may trigger fusion.

Ca^{2+} signaling in skeletal muscle is also very fast. An action potential triggers a sequence of rapid events that results in Ca^{2+} release from intracellular stores within a few milliseconds. Activation of the contractile proteins by the Ca^{2+} ions and force generation occur shortly thereafter. During an action potential, depolarization of the transverse tubular system is thought to induce Ca^{2+} release predominantly from the terminal cisternae of the sarcoplasmic reticulum, a highly specialized reticular network that serves as the principal intracellular Ca^{2+} store (Winegrad, 1970; Somlyo et al., 1981). This hypothesis was first suggested by the distribution of Ca^{2+} determined autoradiographically (Winegrad, 1970) and the distribution of the Ca^{2+} release channels (Franzini-Armstrong, 1975), and received strong support from electron-probe microanalysis of ultrathin cryosections, which showed that there were large (60%) decreases in the total Ca^{2+} of the terminal cisternae after tetanic stimulation (Somlyo et al., 1981). Modeling of this localized Ca^{2+} release by calculating the effects of Ca^{2+} binding proteins and diffusion predicts the formation of intrasarcomeric Ca^{2+} gradients that last 10–20 ms before equilibrating within the sarcomere (Cannell and Allen, 1984). In spite of the fundamental importance of Ca^{2+} signaling in excitation-contraction coupling, the hypothesized presence of Ca^{2+} gradients remains unverified because current imaging techniques are not capable of the temporal resolution required for measuring the predicted Ca^{2+} gradients.

Thus, with conventional imaging techniques, the type of Ca^{2+} signals that occur in response to the brief depolarization of an action potential are either missed entirely or captured at late stages when Ca^{2+} ions have already filled most of the cytosol. It is clear that, for detection of such Ca^{2+} signals, an instrument capable of millisecond time resolution and submicron spatial resolution is required. Temporal resolution is conventionally obtained by triggering an event and taking

Received for publication 28 February 1994 and in final form 17 May 1994.
Address reprint requests to Dr. Julio M. Fernandez, Mayo Clinic, Department of Physiology and Biophysics, Medical Sciences Building, 1–117, Rochester, MN 55905; Tel: 507-284-0423; Fax: 507-284-0521; E-mail: camrud@mayo.edu.

0006-3495/94/08/505/10 $2.00

measurements as rapidly as possible thereafter. For imaging experiments this approach is severely limited by the speed of the cameras and other hardware. An alternative approach is to take a single measurement from a series of successive events, each image delayed differently with respect to the event trigger. As long as the response can be reproduced consistently, very high time resolutions can be obtained. Using this approach with a pulsed laser imaging system, Kinosita and colleagues obtained sub-microsecond temporal resolution using potentiometric dyes: the pulsed laser provided the high intensity epi-illumination necessary to obtain a fluorescent image with good signal-to-noise characteristics and the short duration of the illumination allowed the capture of a "snapshot" of the fluorescence from indicator molecules excited during the light pulse (Kinosita et al., 1988; Hibino et al., 1991). Here we describe the use of a pulsed laser fluorescent microscope for measurement of Ca^{2+} gradients in single excitable cells. We have used the method to measure the development and decay of Ca^{2+} gradients in bovine adrenal chromaffin cells and frog skeletal muscle fibers, two model systems commonly used to study stimulus-secretion and excitation-contraction coupling, respectively.

MATERIALS AND METHODS

Pulsed laser Ca^{2+} imaging

The imaging system consisted of an inverted epifluorescence microscope (model IM-35, Carl Zeiss, Oberkochen, Germany), a peltier-cooled charge coupled device (CCD) camera (model C200, Photometrics Ltd., Tucson, AZ) with a 1024 × 1000 pixel CCD chip (model TI 215–30, Texas Instruments, Lubbock, TX), and a host microcomputer (Compaq Desk Pro 386/25, Compaq Computer Corp., Houston, TX) to control image acquisition and image processing using a Mercury array processor (model MC 3200, Mercury computer systems, Inc., Lowell, MA) as previously described (Monck et al., 1992). To this we added a high intensity pulsed coaxial flash lamp dye laser (LumenX model LS-1400, Phase-R Corporation, New Durham, NH), to provide short (350 ns) high intensity pulses of illumination (Kinosita et al., 1988), and a patch-clamp setup composed of a List EPC-7 patch-clamp amplifier and an Indec IDA15125 interface for data acquisition and synchronization of the laser with the Ca^{2+} current measurements. The reproducibility of the laser intensity for successive pulses was better than 2%, as measured from fluorescence of rhod-2 in internal solution (see below for composition). The laser was coupled with a liquid light guide (UV-VIS Liquid Light Guide, 5 mm diameter, 0.47 N.A.; Oriel Corporation, Stratford, CT) to the epifluorescence port of the microscope using a custom built adapter with a fused silica plano-convex lens (1 inch diameter, F/2; Oriel) positioned 2 inches from the end of the light guide, so that the entire field of view was illuminated. The lasing dye, Coumarin 521 (0.02 mM in methanol), gave a suitable emission spectrum (500–540 nm) for excitation of rhod-2. The epifluorescence filter block contained a 570 nm DRLP dichroic mirror and 585 nm EFLP emission filter (Omega Optical, Brattleboro, VT). Zeiss 100X (N.A. 1.3) and 40X objectives (0.65 N.A.) were used to image muscle fibers and chromaffin cells, respectively. Image pairs were taken for control and depolarizing pulses.

Image processing

Where indicated (see Figs. 2 and 6), the images were filtered using an inverse filter designed to remove out-of-focus light. The "no neighbors" deblurring filter is essentially a high pass filter that selectively removes the lower spatial frequencies associated with out-of-focus light and, consequently, corrects for the low pass filtering effect of the microscope optics (Monck et al., 1992). The theoretical point spread function for the objective is used to determine the filter characteristics. The filter was derived from the nearest neighbors filter, which uses an image plane above and below to estimate the out-of-focus light in an image. We have previously shown that the no-neighbors filter gives deblurring almost indistinguishable from that of the nearest neighbors technique (Monck et al., 1992). This is because the out-of-focus light estimated from the in-focus plane is almost the same as that estimated from the neighboring planes. The deblurring algorithm is as follows:

$$I_j = \{O_j - 2cO_jS_1\}G \quad (1)$$

where O_j is the two-dimensional Fourier transform of the observed image; I_j the restored in-focus image, S_1 is the out-of-focus contrast transfer function (the Fourier transform of the point spread function), and c an empirical constant that determines the amount of deblurring applied. G is a Wiener inverse filter of the form $G = S_0/(S_0^2 + \alpha)$, where S_0 is in-focus contrast transfer function and α is an empirical constant. The Wiener filter is a noise reduction filter; the best value for α depends upon the total signal and signal to noise of the images (typical values are in the range 0.5–5.0, increasing values give increased smoothing). Because the properties of the objective dominate the transfer function of the microscope, we use theoretical contrast transfer functions for the objective to calculate S_0 and S_1 using the equations given by Agard (1984). For calculating S_1 we assume a section spacing (Δz) which serves to control the thickness of the optical sections. Thus, the parameters Δz and c determine the extent of the deblurring (see Monck et al. (1992) for details). Good deblurring uses settings in the range 0.5 μm to 1 μm for Δz and 0.48 to 0.50 for c, but this requires a relatively high intensity image. Other parameters for calculating S_0 and S_1 are the numerical aperture of the objective lens, the wavelength of emitted light (600 nm), pixel size, and the index of refraction of the objective immersion oil. The filter parameters in Fig. 2 were $\Delta z = 2$ μm, $c = 0.45$, $\alpha = 5$, numerical aperture = 0.65, pixel size = 133 nm. Note that this does not give optimal deblurring, which would have required an image with a higher intensity. The filter parameters in Fig. 6 were $\Delta z = 2$ μm, $c = 0.49$, $\alpha = 3$, numerical aperture = 1.3, and pixel size = 62.5 nm. The chromaffin cell images in Figs. 3 and 4 were filtered to reduce the noise before calculating the ratio: the filter parameters ($\Delta z = 2$ μm, $c = 0.2$, and $\alpha = 5$) were set to remove the highest frequencies (i.e., the noise) with minimal deblurring characteristics (i.e., the estimated Ca^{2+} concentrations were the same after filtering as before filtering). Similar noise reduction could be obtained using a 3 × 3 spatial filter with all the elements set to unity. The inverse filtering usually introduces some negative values into the images. Therefore, we applied a threshold operation to set negative values to 0 (i.e., a non-negativity constraint).

Ca^{2+} concentration estimates

For the chromaffin cells, the ratio of the stimulus image divided by the control image is displayed as a pseudo-color image representing the fractional change in fluorescence. Since the ratio corrects for differences in indicator concentration, indicator excluded volume and light path length, the fractional change in fluorescence represents a measure of the Ca^{2+} change, provided that the cell does not move between the control and stimulus image. Rhod-2 does not undergo a shift in either excitation or emission spectra on binding Ca^{2+}, so we cannot use a ratiometric calibration ((Minta et al., 1989). Instead, the change in Ca^{2+} concentration was estimated from the fractional fluorescence change (stimulus/control ratio), as described previously (Monck et al., 1988), using 1300 nM for K_d and 0.005 for α (the ratio of the fluorescence of free and Ca^{2+} bound rhod-2, determined in vitro using internal solution with "zero" Ca^{2+} (10 mM EGTA) and saturating Ca^{2+} (10 mM Ca^{2+}, 10 mM EGTA), respectively). Using a resting value of 100 nM for the resting Ca^{2+} concentration, this gives peak Ca^{2+} concentrations of around 200 nM. In general, estimates of the resting free Ca^{2+} in the range 50–200 nM give peak Ca^{2+} increases of about 2- to 2.5-fold. Since most of the fluorescence signal comes from the Ca^{2+} bound form of rhod-2, the Ca^{2+} estimates are relatively insensitive to the value of α used, so provided the in situ value of α is less than 0.05 the estimates of Ca^{2+} remain accurate. For the skeletal muscle fibers the K_d and α determined in the intracellular

solution were 1300 nM and 0.007, respectively (Escobar et al., 1994). Because of the large fractional change in fluorescence (six- to sevenfold in Fig. 6) in the muscle fibers, the calculated value for the peak Ca^{2+} concentration is more sensitive to the estimate of the resting Ca^{2+} concentration (for ratio = 6: 100 nM for the resting gives 1.1 μM for the peak, 150 nm gives 2.5 μM and 200 nM gives 6.6 μM). These values are similar to the values reported in frog skeletal muscle by others (1–10 μM, depending on Ca^{2+} indicator; see Konishi et al., 1991 for discussion).

Adrenal chromaffin cells

Chromaffin cells were prepared from bovine adrenal medullae by enzymatic digestion (Burgoyne et al., 1988). Isolated cells were resuspended in Dulbecco's modified Eagle's medium supplemented with 25 mM HEPES, 10% fetal calf serum, 8 μM fluorodeoxyuridine, 50 μg/ml gentamycin, 10 μM cytosine arabinofuranoside, 2.5 μg/ml fungizone, 25 U/ml penicillin, and 25 μg/ml streptomycin and plated at a density of 100,000 cells/ml on glass-bottomed chambers. Cells were kept 1–7 days in culture before use. For experiments, cells were washed in an extracellular medium composed of 120 mM NaCl, 20 mM HEPES, 4 mM $MgCl_2$, 5 mM $CaCl_2$, 4 mg/ml glucose, and 1 or 2 μM tetrodotoxin (pH 7.25). The internal solution used in the patch-clamp pipettes contained 125 mM Cs D-glutamate, 30 mM HEPES, 8 mM NaCl, 1 mM $MgCl_2$, 2 mM Mg-ATP, 0.3 mM GTP, 0.3 mM Cs-EGTA, and 0.2 mM rhod-2 (triammonium) (pH 7.2). These solutions allow measurement of Ca^{2+} currents because Na^+ and K^+ currents are prevented. The holding potentials have not been corrected for junction potentials, which means that, for the Cs^+-glutamate based solution used here, the actual holding potentials are 10–12 mV more negative (Neher, 1993).

Frog skeletal muscle fibers

An inverted double vaseline gap technique was used for simultaneous electrical recording of induced action potentials and high resolution Ca^{2+} imaging (Escobar et al., 1994). Single skeletal muscle fibers were dissected from the semitendinosus muscle of the bullfrog *Rana catesbeiana*. Short segments (2–3 mm) of muscle fibers were extended on thin coverslips which formed the bottom of a double vaseline gap chamber and stretched to sarcomere spacings of 3.8–4.0 μm. The ends of the muscle fibers at the lateral pools were fixed to the bottom of the chamber with adhesive tape. A Teflon molding with three holes and two small partitions was placed over the coverslip to separate three pools that were electrically connected (by agar bridges) to an electronic circuit for stimulation of the muscle fiber in a current clamp configuration. The ends of the fibers within the lateral pools were permeabilized with saponin (200 μg/ml) to allow for diffusion of solutes into the myoplasm. The two lateral pools were then filled with an internal solution containing: 110 mM K-aspartate; 20 mM K-MOPS; 5 mM Na_2-PCr, 5 mM Na_2-ATP, 150 μM EGTA, 3 mM $MgCl_2$, 0.1 mg/ml creatine kinase, and 300 μM rhod-2 (pH 7.0, 245 mOsm). The fibers were externally perfused in the central pool with Ringer's solution at about 15°C.

RESULTS

Pulsed laser imaging for rapid Ca^{2+} imaging

To study the kinetics of Ca^{2+} gradients we needed an imaging system capable of high temporal and spatial resolution. We assembled a pulsed laser imaging system comprising a direct-readout, cooled CCD camera and a high power coaxial flashlamp dye laser, as shown in Fig. 1. The cooled CCD camera is a lag-free, low noise imaging device which efficiently accumulates charge in each element of the CCD chip in proportion to the number of incident photons (Hiraoka et al., 1987). A transient high intensity illumination from the pulsed laser allows us to capture a "snapshot" of the fluorescence from indicator molecules excited during the 350-ns duration of the laser pulse (Kinosita et al, 1988). We synchronized firing of the laser pulse with the opening of voltage-sensitive Ca^{2+} channels in cells loaded with the fluorescent Ca^{2+} indicator rhod-2, and were able to obtain snapshots of the Ca^{2+} distribution at known times after the depolarizing stimulus. Time courses were built up by taking a series of images for successive depolarizing stimuli, each delayed differently with respect to the event trigger.

Ca^{2+} gradients develop at discrete submembrane domains in adrenal chromaffin cell

Fig. 2 shows a pair of fluorescent images taken of a chromaffin cell kept at the holding potential of −60 mV (control)

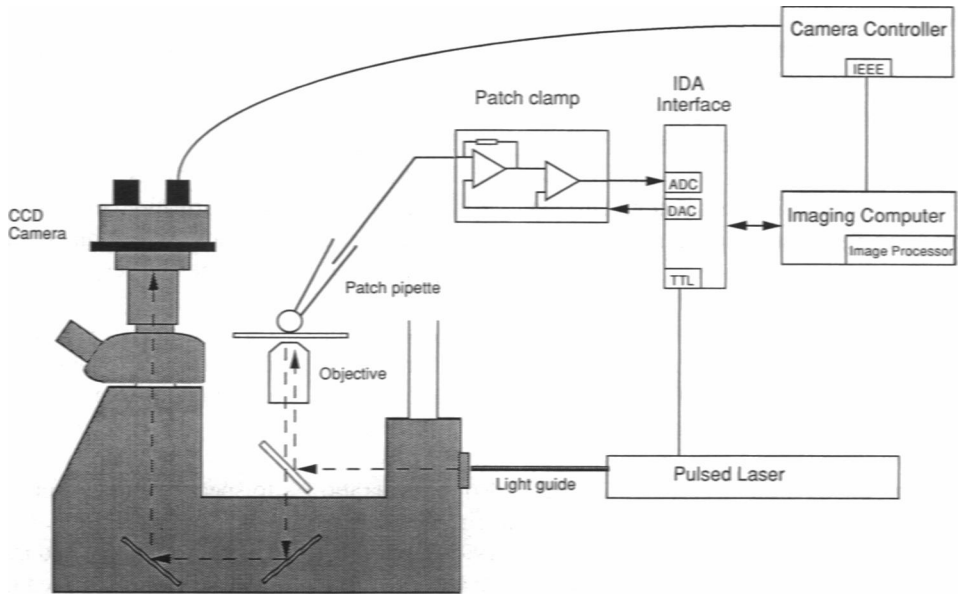

FIGURE 1 Schematic of the pulsed-laser imaging system used to measure Ca^{2+} gradients with high temporal and spatial resolution. The essential components are as follows: an inverted microscope; a cooled CCD camera as the detector; a high intensity pulsed coaxial flash lamp dye laser to provide short (350 ns) high intensity pulses of illumination; an image processor for digital deblurring of the images; and a patch clamp setup.

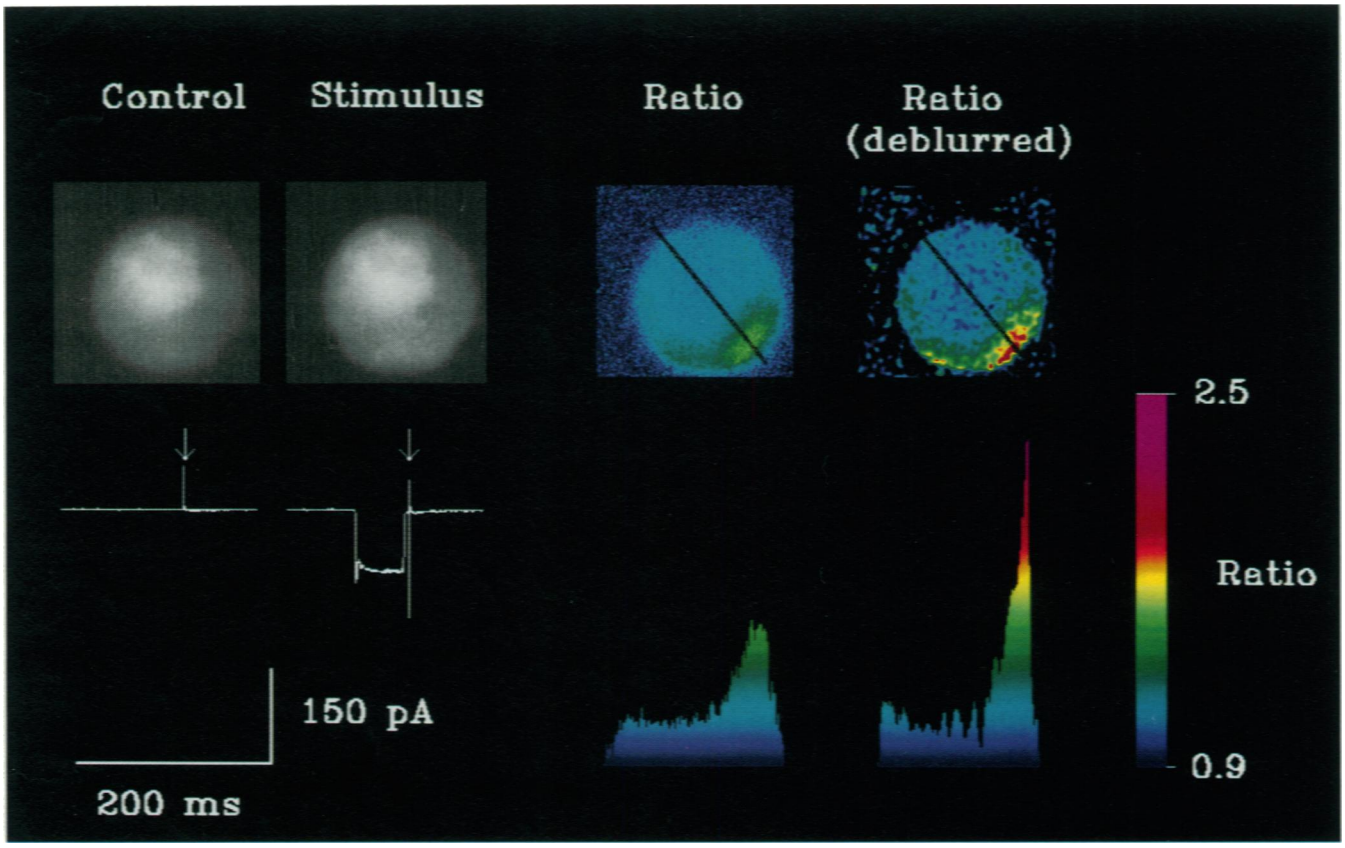

FIGURE 2 Fast Ca^{2+} imaging in adrenal chromaffin cells. Images of rhod-2 loaded chromaffin cells were taken 5 ms after the end of a 50-ms depolarization to +20 mV (stimulus) or without a depolarization (control). Holding potential, −60 mV. Below each image are the corresponding Ca^{2+} currents. The arrows marked the time of the laser discharge. Images are averages of three depolarizations (2 s apart). The ratio of the stimulus and control images is displayed in pseudocolor and clearly shows the localization of the Ca^{2+} increase. The pipette was located at 3 o'clock. The profile follows the line through the image. The figure also shows that application of a digital deblurring filter, designed to remove out-of-focus light, causes a sharpening of the Ca^{2+} gradient.

and then 5 ms after the end of a 50-ms depolarization to +20 mV (stimulus). The corresponding traces of membrane current show that this depolarization protocol induced a non-inactivating Ca^{2+} current, which had a voltage dependence similar to that previously demonstrated (Fenwick et al., 1982; Artalejo et al., 1991). The spike artifact in the current trace indicates when the laser was fired. Although an increase in fluorescence attributable to a Ca^{2+} increase can be seen in the raw images, the precise distribution of the Ca^{2+} change is obscured because of differences in light path length, indicator concentration, and volume occupied by the indicator. When these differences are compensated for ratiometrically, by dividing the stimulus image by the control image, it can be clearly seen that the Ca^{2+} increase is spatially restricted to a region just beneath the plasma membrane located at about 4 o'clock, and that the increase over the remainder of the cell is considerably smaller. From the fluorescence change, we can estimate a Ca^{2+} increase from 100 nM to 200 nM at the hot spot. However, the out-of-focus light that appears in fluorescence images causes attenuation of observed Ca^{2+} gradients (Monck et al., 1992). Fig. 2 also shows a ratio image obtained after applying a digital deblurring filter to the control and stimulus images (Monck et al., 1992). From this image we estimated a peak Ca^{2+} concentration of about 300 nM, indicating that the Ca^{2+} gradient is in the range 25–50 nM/μm.

Different patterns of localized Ca^{2+} elevation were seen in different cells, but the pattern in each cell was reproducible. Many cells had discrete hot spots of elevated Ca^{2+} in one or more locations around the cell periphery, whereas in other cells the hot spots had merged into partial rings (Fig. 3). In all cases, the increases were largest immediately beneath the plasma membrane. In general, hot spot patterns were seen for depolarizations of 50 ms or shorter, whereas complete rings of elevated Ca^{2+} were seen for longer depolarizations. The reproducibility of the Ca^{2+} response allows us to acquire time courses by taking a series of images where the delay between depolarization and the trigger for the laser is varied.

The Ca^{2+} gradients develop relatively slowly compared with the Ca^{2+} currents. Fig. 4 shows a typical example. Very little change in Ca^{2+} was apparent 10 ms after opening the Ca^{2+} channels. After 20 and 30 ms, a highly localized gradient appeared at about 1 o'clock. There was some indication of smaller increases in Ca^{2+} elsewhere around the perimeter of the cell, but no significant increases in the cell interior. Thus for short depolarizations the Ca^{2+} stimulus is restricted to specific regions beneath the cell membrane. At 55 ms, 5 ms after termination of the pulse, the gradient in the original location has increased in magnitude and breadth and there is a clear ring of elevated Ca^{2+} around the entire perimeter, as well as a smaller increase in the centre of the cell. The change

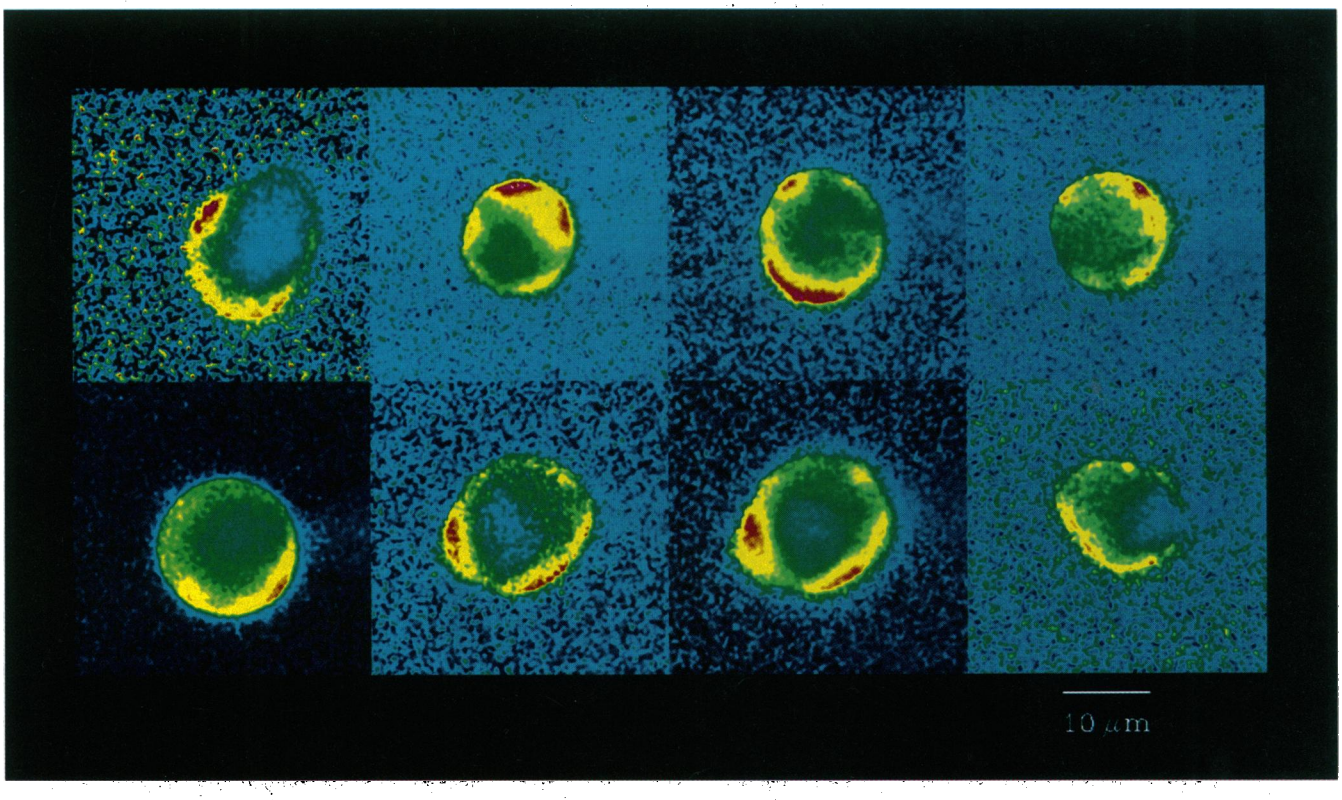

FIGURE 3 Spatial distribution of Ca^{2+} gradients in chromaffin cells. Examples showing different patterns of Ca^{2+} elevations in different cells. All images are ratios for stimulus and control images taken 5 ms after a 50-ms depolarization to +20 mV. All images are averages of three control-stimulus pairs (2 or 3 s apart), except for *vi* which is a "single shot" image of the cell shown in *vii*. The pipette is located on the right in all cases.

in fluorescence integrated over the whole cell increased linearly with pulse duration and showed no non-linearities that might indicate intracellular Ca^{2+} release. At the end of the depolarizing pulse the Ca^{2+} gradients collapsed over several hundred milliseconds, leaving a spatially uniform Ca^{2+} increase, as indicated by the images taken 200 and 400 ms after the beginning of the pulse (Fig. 4).

Intrasarcomeric Ca^{2+} gradients in frog skeletal muscle

Considerably faster and larger gradients were observed within individual sarcomeres in frog skeletal muscle. Single muscle fibers were mounted in an inverted vaseline gap chamber and stretched to prevent contraction (Escobar et al., 1994). Depolarization under current clamp elicited an action potential (Fig. 5 *A*), during which the sarcomeric length was unchanged. An image taken without an action potential shows a low and featureless background fluorescence (Fig. 5 *C*, control). No changes were observed during the first 3 ms following onset of the action potential, consistent with the 3 ms triadic delay for the Ca^{2+} transient (Vergara and Delay, 1986), but at 3.5 ms a change in fluorescence with a banded pattern was observed (Fig. 5 *C*). The bands became more pronounced at 5 ms, whereas at longer times (> 10 ms) the fluorescence became homogeneous (Fig. 5 *C*). The spacing of the fluorescence bands corresponded to the sarcomere length (Fig. 5 *B*). In experiments using the confocal spot technique to measure the kinetics of the Ca^{2+} increases from micron diameter spots positioned either at the Z-line or M-line, the largest and fastest increases were shown to occur over the t-tubules (Escobar et al., 1994). In these experiments the location of the t-tubules was confirmed by staining the muscle fibers with RH-795, a potentiometric dye. Fig. 6 shows the time course in another muscle fiber. For this fiber, the data is displayed as ratio images after filtering with a digital deblurring algorithm (Monck et al., 1992) to obtain a more accurate image of the Ca^{2+} distribution within a sarcomere (Fig. 6). Below each image are the corresponding intensity profiles through three sarcomeres, which show steeper Ca^{2+} gradients than suggested by the unprocessed images. The rapid appearance of the Ca^{2+} gradient between 2.8 and 3 ms (Fig. 6), equivalent to a Ca^{2+} increase to about 600 nM in 200 μs, is faster than in chromaffin cells, where 300 nM is attained only after a 50-ms depolarization (Figs. 2 and 4). This faster Ca^{2+} increase in the muscle fiber is presumably due to the massive release from the terminal cisternae of the sarcoplasmic reticulum.

DISCUSSION

Temporal and spatial limitations of pulsed laser Ca^{2+} imaging

The results presented in this paper clearly demonstrate that pulsed laser imaging techniques can be used to measure Ca^{2+} gradients with millisecond time resolution, while retaining the maximum spatial resolution attainable with fluorescent

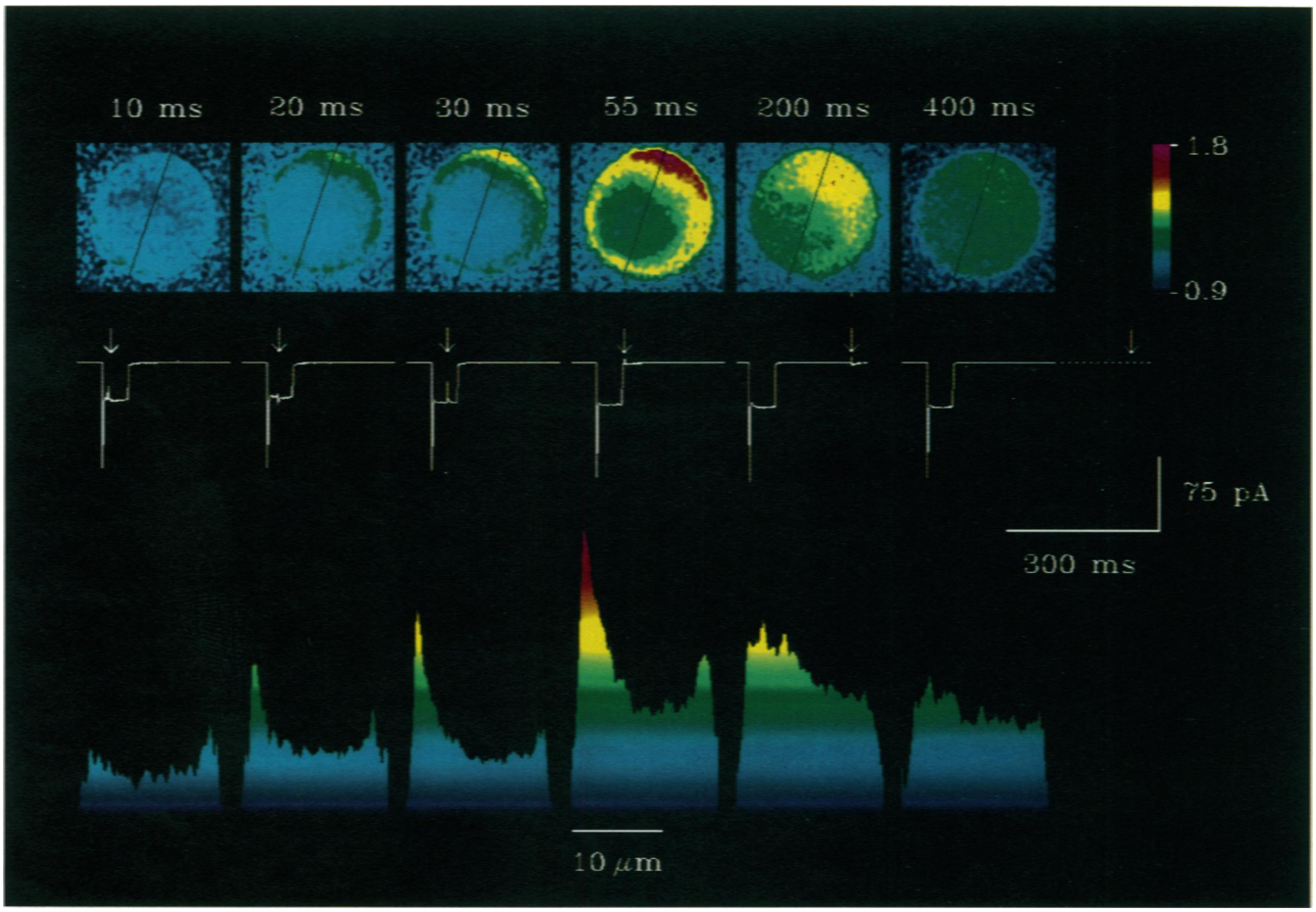

FIGURE 4 Time-course of Ca^{2+} gradients development in response to opening of Ca^{2+} channels in chromaffin cells. (*A*) Sequence of ratio images taken following different time delays (10–400 ms, marked by the arrows), measured from the beginning of a pulse of 50 ms duration from −60 mV to +20 mV. The profiles (*bottom*) show the ratio values along the lines through the images (*top*). Note that the peak of Ca^{2+} gradient increases throughout the duration of the depolarization and the gradients dissipate over hundreds of milliseconds after the end of the pulse.

microscopy. The two key components of the system are the pulsed coaxial flash-lamp dye laser and the cooled CCD camera. The pulsed laser is used to illuminate the entire field of view. The high intensity of the laser pulse provides sufficient illumination to obtain a good emission intensity, and the short duration provides a snapshot of the fluorescence from the indicator excited within the pulse length, in this case 350 ns. The duration of the snapshot will also include the lifetime of the excited state of the indicator after the pulse. However, for BAPTA series fluorescent indicators the lifetime is very short (2 ns for Fura-2; Keating and Wensel, 1991). The slow readout rate of the CCD camera does not affect the time resolution because the CCD only receives photons during the laser pulse (and shortly, thereafter); there is negligible background detected during the readout time because of the excellent noise characteristics of the camera. Instead, time courses must be built up by repeating the stimulus with different delays before triggering the laser. Thus, the important requirement for this approach is a physiological response that is highly reproducible.

The experiment in Fig. 6 clearly shows the appearance of a Ca^{2+} gradient over a 200-μs time interval (2.8–3 ms). The time limitation on the pulsed laser imaging technique is determined by the length of the laser pulse (350 ns for the Phase-R LS1400 laser used here) and the kinetic properties of the fluorescent indicator. For BAPTA-series Ca^{2+} indicators, such as Fura-2 or rhod-2, the conventional Ca^{2+} calibration procedures assume that Ca^{2+} and the Ca^{2+} indicator are in equilibrium. For these dyes equilibration times are of the order of milliseconds (Lattanzio and Bartschat, 1991). Thus, for the measurements in chromaffin cells and the decay phase of the muscle Ca^{2+} transients, the rhod-2 would have been in equilibrium. On the other hand, the indicator would not have been in equilibrium during the rapid increase in the muscle fibers, resulting in an underestimate of the free Ca^{2+} concentration. Because the on-rate constant for Ca^{2+} binding is $>10^8\ M \cdot s^{-1}$ (Lattanzio and Bartschat, 1991), the BAPTA-series indicators are sensitive to much faster changes in Ca^{2+} concentration. However, novel kinetic calibration procedures will need to be developed to calculate the free Ca^{2+} concentration. Measurements using fluorescence probes for other cellular parameters are not necessarily subject to these limitations. For example, Hibino et al. (1991) have successfully measured changes in transmembrane potential with submicrosecond time resolution.

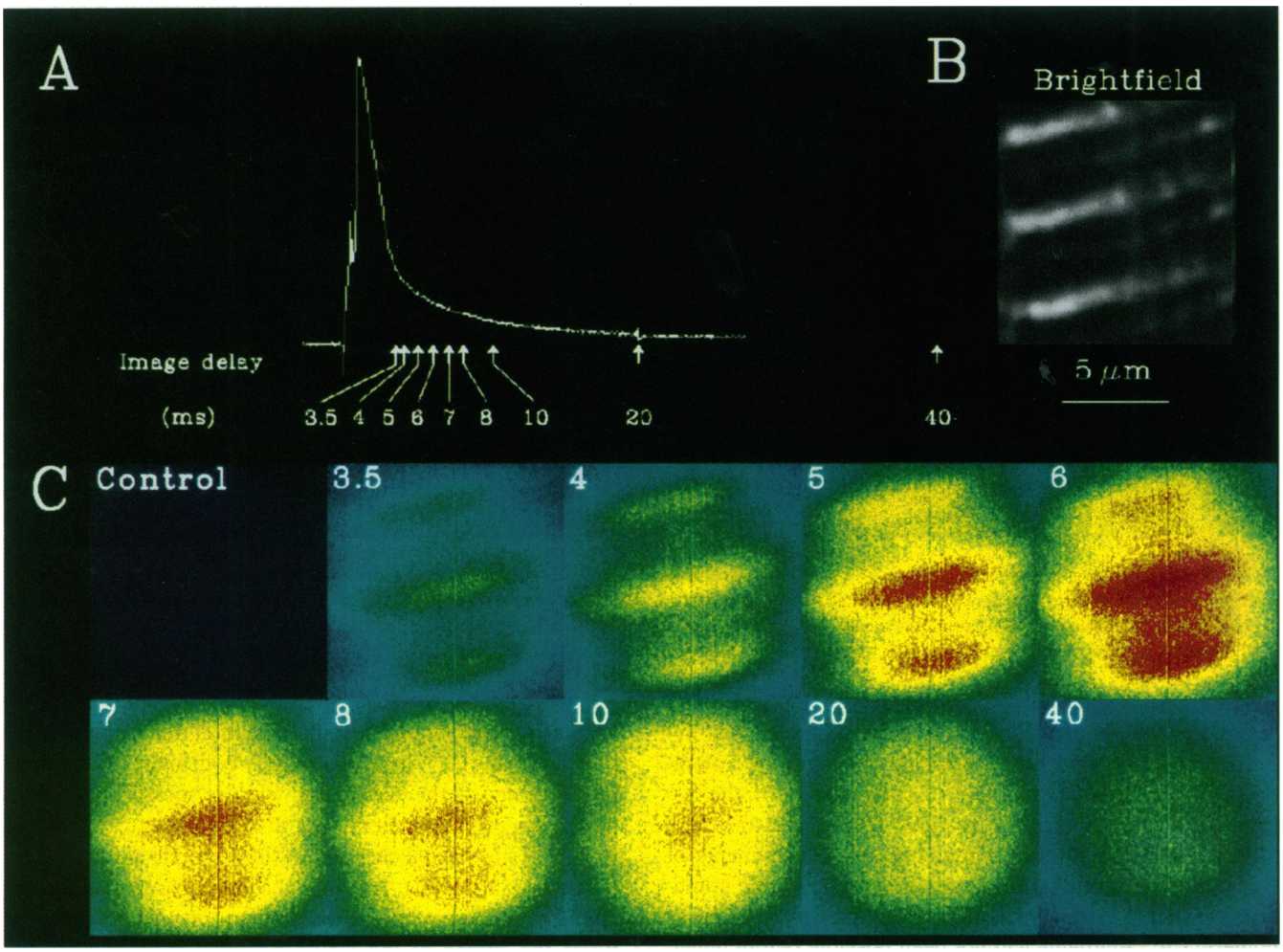

FIGURE 5 Intrasarcomeric Ca^{2+} gradients in frog skeletal muscle fibers. Fibers were held at −90 mV in current clamp. (*A*) Depolarization induced an action potential. (*B*) Bright field image showing sarcomere structure. (*C*) Fluorescence images from rhod-2 loaded fibers taken after delays of 3.5, 4, 5, 6, 7, 8, 10, 20, 25, and 40 ms, respectively (marked by arrows in *A*).

Several other approaches to improve temporal resolution of imaging experiments have been made. These range from using conventional video equipment at the maximum possible rate (17 ms/frame; Takamatsu and Wier, 1990) to using CCD arrays with reduced spatial resolution or reduced area of interest, and using CCD cameras in frame transfer mode, which has been successful at measuring Ca^{2+} transients in cardiac myocytes with 10 ms temporal resolution (O'Rourke et al., 1990). The scanning confocal microscope has been used in line-scan mode to measure Ca^{2+} gradients in bullfrog sympathetic neurons (Hernandez-Cruz et al., 1990; Nohmi et al., 1992) and rat hippocampal neurons (Segal and Manor, 1992). The results reveal Ca^{2+} gradients that slowly develop over hundreds of milliseconds, similar to the results in chromaffin cells, reported here. However, although the line scan mode can have a temporal resolution of about 4 ms, the signal to noise is not good enough to examine the gradients after only a few milliseconds. A disadvantage of the confocal line scan method is that information is only obtained in one dimension. On the other hand, the confocal line scan can be used to measure the time course of a one-shot event, whereas the pulsed laser imaging only obtains a single snapshot and requires a reproducible response to build up a time course.

A major advantage of pulsed laser imaging is that temporal resolution is not gained at the expense of spatial resolution. For example, the Ca^{2+} gradients measured in the frog skeletal muscle fibers used a 1.3 N.A. objective, which has a potential maximum spatial resolution of about 0.2 μm. In the current experiments, the images include contamination with out-of-focus light, which effectively reduces the spatial resolution. However, digital deblurring techniques can reduce the contamination with out-of-focus light, as shown for chromaffin cells in Fig. 2 and for a muscle fibers in Fig. 6. Alternatively, because the response to each action potential is highly reproducible, it would be possible to perform optical sectioning on the cells and obtain a three-dimensional data set for reconstruction of a three dimensional image (Agard et al., 1989; Fay et al., 1989).

Intrasarcomeric Ca^{2+} gradients in frog skeletal muscle

The experiment shown in Fig. 3 demonstrates the measurement of an intrasarcomeric Ca^{2+} gradient in skeletal muscle and provides further evidence that the action potential induced Ca^{2+} release comes predominantly from the terminal

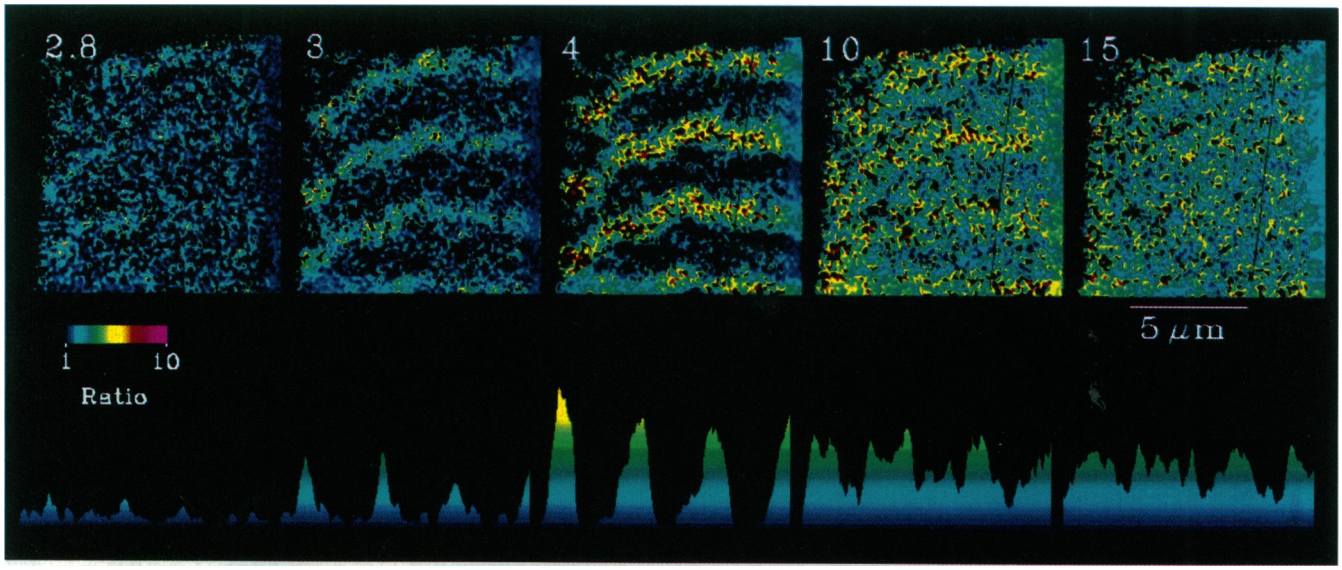

FIGURE 6 Ratio images of intrasarcomeric Ca^{2+} gradients in frog skeletal muscle fibers. Images were obtained from another muscle fiber and filtered with the no-neighbors algorithm to reduce contamination by out-of-focus light. Pairs of images were taken 2.8, 3, 4, 10, and 15 ms after onset of the depolarization. The ratios were averages of four control-stimulus pairs (5 s apart). Below each ratio image is the corresponding profile through the line marked on the image. To reduce the noise, the profiles were further filtered with a 9 × 9 spatial filter with all elements set to unity.

cisternae of the sarcoplasmic reticulum. Although this hypothesis is supported by experiments showing the autoradiographic distribution of $^{45}Ca^{2+}$ (Winegrad, 1970), the distribution of the Ca^{2+} release channels (Franzini-Armstrong, 1975), and electron-probe microanalysis measurements of the total Ca^{2+} in the terminal cisternae after tetanic stimulation (Somlyo et al., 1981), direct visualization of intrasarcomeric Ca^{2+} gradients had not been possible before development of the pulsed laser Ca^{2+} imaging technique shown here. The demonstration that intrasarcomeric Ca^{2+} gradients form rapidly and last less than 10 ms before the Ca^{2+} concentration becomes homogeneous within the sarcomere (Fig.5) fits reasonably well with a model of Ca^{2+} release and diffusion within individual sarcomeres where the Ca^{2+} gradient was predicted to last 10–20 ms (Cannell and Allen 1984).

The Ca^{2+} gradient in skeletal muscle fibers develops very rapidly. The experiment in Fig. 6 clearly shows a Ca^{2+} gradient that became apparent between 2.8 and 3 ms. During this 200 μs interval, the Ca^{2+} increased by about 500 nM. This rapid Ca^{2+} increase in the muscle fiber is presumably due to the massive release from the terminal cisternae of the sarcoplasmic reticulum, where the Ca^{2+} current density is estimated at >200 pA μm^{-2} (Franzini-Armstrong, 1975). Although Fig. 5 seems to indicate that the Ca^{2+} concentration also increases rapidly in center of the sarcomere, it is possible the fluorescence increase in the center of the sarcomeres could come from out-of-focus light from underlying t-tubules. As shown in Fig. 6, there appears to be little increase in Ca^{2+} between the t-tubules for the first few milliseconds after Ca^{2+} release when a digital deblurring filter is used to reduce out-of-focus information. However, the signal to noise in this experiment makes it difficult to exclude a small Ca^{2+} increase at the M line. Experiments using the confocal spot technique to measure high resolution time courses have shown that the Ca^{2+} increases rapidly both at the t-tubule and in the center of the sarcomere, with no measurable delay, which suggests that there may also be some Ca^{2+} release from the longitudinal cisternae of the sarcoplasmic reticulum (Escobar et al., 1994). Together, the pulsed laser imaging and confocal spot techniques provide the tools to further investigate the spread of the action potential-induced Ca^{2+} increases within single sarcomeres.

Localized Ca^{2+} gradients in adrenal chromaffin cells

In chromaffin cells, standing gradients of Ca^{2+} slowly develop at discrete domains beneath the cell membrane. Although Ca^{2+} changes restricted to 5- to 20-μm regions of neuronal processes have been observed experimentally (Silver et al., 1990; Regyhr and Tank, 1990; Guthrie et al., 1991; Muller and Connor, 1991), this is the first report of such highly localized Ca^{2+} influx in small round cells. One factor responsible for the restriction of the Ca^{2+} increase to discrete submembrane domains could be that the Ca^{2+} channels activated by depolarization are preferentially localized in these regions of the plasma membrane. Clustering of Ca^{2+} channels has previously been reported in several cell types (Westenbroek et al., 1990; Robitaille et al., 1990), as well as in the active zones of synaptic terminals and saccular hair cells (Smith and Augustine, 1988; Augustine et al., 1991; Roberts et al., 1990). Recent studies using microvoltametry have revealed secreting and non-secreting domains on the surface of chromaffin cells (Shroeder et al., 1994), which raises the interesting possibility that the Ca^{2+} hot spots mark the location of exocytotic sites.

Previous studies on adrenal chromaffin cells have reported complete rings of elevated Ca^{2+} around the cell periphery approximately 100 ms after the onset of a depolarizing stimulus (O'Sullivan et al., 1989; Cheek et al., 1989; Neher and Augustine, 1992). Our results, showing that for short depolarizations the Ca^{2+} stimulus is restricted to specific regions beneath the cell membrane, do not contradict those observations since the hot spot patterns seen for short (<50 ms) depolarizations, typically develop into complete rings after longer depolarizations. It has generally been assumed that the rings seen at late times represent temporally low-pass filtered remnants of much larger, earlier elevations of Ca^{2+} in the 10–100 μM range, as predicted by Ca^{2+} modeling studies (Sala and Hernandez-Cruz, 1990; Nowycky and Pinter, 1993). In contrast, our results show that Ca^{2+} gradients develop over 10–50 ms and that the observed Ca^{2+} changes are small. Only after opening the Ca^{2+} channels for 50 ms does the Ca^{2+} concentration at the hot spot reach 300 nM.

The presence of maintained Ca^{2+} gradients indicates that the movement of Ca^{2+} ions entering the cell is restricted, since diffusion of free Ca^{2+} (or Ca^{2+} bound to rhod-2) in aqueous solution predicts movement of 1 μm in 1 ms. Zhou and Neher (1993) have shown that chromaffin cells have substantial amounts of immobile Ca^{2+} buffers, enough to reduce the effective diffusion coefficient to 0.1×10^{-6} cm^2 s^{-1} (or about 0.15 μm in 1 ms). Maintained Ca^{2+} gradients develop in the presence of immobile Ca^{2+} binding sites because preferential binding to the immobile sites restricts diffusion of free Ca^{2+} to the cell interior (Sala and Hernandez-Cruz, 1990; Nowycky and Pinter, 1993). These models predict that the presence of the indicator results in some spreading of the gradient due to diffusion of the Ca^{2+}-indicator complex, which suggests that, in the absence of the indicator, the gradients might remain even more spatially localized. However, predicting the effects of the indicator is further complicated by the possibility that a substantial fraction of the rhod-2 might be bound, as has been reported for Fura-2 (Konishi et al., 1988), and that mobile Ca^{2+} buffers such as calbindin, a small Ca^{2+} binding protein, are found in some cells (Roberts, 1993), although chromaffin cells do not have large amounts of endogenous mobile Ca^{2+} buffers (Zhou and Neher, 1993). Nevertheless, the ability, as described here, to measure Ca^{2+} gradients simultaneously at high spatial and temporal resolution in small excitable cells, along with the advent of new membrane anchored Ca^{2+} indicators (Etter et al., 1994), offers the opportunity to investigate the interaction between local Ca^{2+} entry and cytosolic buffering, and how these factors interact to regulate exocytosis.

CONCLUSION

Ca^{2+} signaling in millisecond time scales underlies the physiological response to action potentials in excitable cells. We have used pulsed laser Ca^{2+} imaging to measure the time courses of the development and decay of Ca^{2+} gradients in chromaffin cells and skeletal muscle fibers. The pulsed laser imaging method was successful because it is not limited by the poor temporal and/or spatial resolution of other imaging techniques. This approach can be readily adapted to study cellular responses to rapid photolysis of caged compounds (Ca^{2+}, IP_3, ATP, neurotransmitters) or to the capture of rare and/or transient events.

REFERENCES

Agard, D. 1984. Optical sectioning microscopy: cellular architecture in three dimensions. *Annu. Rev. Biophys. Bioeng.* 13:191–219.

Agard, D. A., Y. Hiraoka, P. Shaw, and J. W. Sedat. 1989. Fluorescence microscopy in three dimensions. *Methods Cell Biol.* 30:353–377.

Artalejo, C. R., M. K. Dahmer, R. L. Perlman, and A. P. Fox. 1991. Two types of Ca^{2+} currents are found in bovine chromaffin cells: facilitation is due to the recruitment of one type. *J. Physiol.* 432:681–707.

Augustine, G. J., E. M. Adler, and M. P. Charlton. 1991. The calcium signal for transmitter secretion from presynaptic nerve terminals. *Ann. N. Y. Acad. Sci.* 635:365–381.

Augustine, G. J., and E. Neher. 1992. Calcium requirements for secretion in bovine chromaffin cells. *J. Physiol.* 450:247–271.

Burgoyne, R. D., A. Morgan, and A. J. O'Sullivan. 1988. A major role for protein kinase C in calcium-activated exocytosis in permeabilised adrenal chromaffin cells. *FEBS Lett.* 238:151–155.

Cannell, M. B., and D. G. Allen. 1984. Model of calcium movements during activation in the sarcomere of frog skeletal muscle. *Biophys. J.* 45: 913–925.

Cheek, T. R., A. J. O'Sullivan, A. J., R. B. Moreton, M. J. Berridge, and R. D. Burgoyne. 1989. Simultaneous measurements of cytosolic calcium, and secretion in single bovine adrenal chromaffin cells by fluorescent imaging of fura-2 in cocultured cells. *FEBS Lett.* 247:429–434.

Douglas, W. W. 1968. The first Gaddum memorial lecture. *Br. J. Pharmacol.* 34:451–474.

Escobar, A. L., J. R. Monck, J. M. Fernandez, and J. L. Vergara. 1994. Localization of the site of Ca^{2+} release at the level of a single sarcomere in skeletal muscle fibres. *Nature.* 367:739–741.

Etter, E. F., M. A. Kuhn, and F. S. Fay. 1994. Detection of changes in near-membrane Ca^{2+} concentration using a novel membrane-associated Ca^{2+} indicator. *J. Biol. Chem.* 269:10141–10149.

Fay, F. S., W. Carrington, and K. E. Fogarty. 1989. Three-dimensional molecular distribution in single cells analysed using the digital imaging microscope. *J. Microsc.* 153:133–149.

Fenwick, E. M., A. Marty, and E. Neher. 1982. Sodium, and calcium channels in bovine chromaffin cells. *J. Physiol.* 331:599–635.

Franzini-Armstrong, C. 1975. Membrane particles, and transmission at the triad. *Fed. Proc.* 34:1392–1389.

Guthrie, P. B, M. Segal, and S. B. Kater. 1991. Independent regulation of calcium revealed by imaging dendritic spines. *Nature.* 354:76–80.

Hernandez-Cruz, A., F. Sala, and P. R. Adams. 1990. Subcellular calcium transients visualized by confocal microscopy in a voltage-clamped vertebrate neuron. *Science.* 247:858–862.

Hibino, M., M. Sigemori, H. Itoh, K. Nagayama, and K. Kinosita, Jr. 1991. Membrane conductance of an electroporated cell analyzed by submicrosecond imaging of transmembrane potential. *Biophys. J.* 59:209–220.

Hiraoka, Y., J. W. Sedat, and D. A. Agard. 1987. The use of a charge-coupled device for quantitative optical microscopy of biological structures. *Science.* 238:36–41.

Keating, S. M., and T. G. Wensel. 1991. Nanosecond fluorescence microscopy. Emission kinetics of Fura-2 in single cells. *Biophys. J.* 59:186–202.

Kinosita K., Jr., I. Ashikawa, M. Hibino, M. Shigemori, H. Yoshimura, H. Itoh, K. Nagayama, and A. Ikegami. 1988. Submicrosecond imaging under a pulsed-laser fluorescence microscope. *SPIE.* 909:271–277.

Konishi, M., S. Hollingworth, A. B. Harkins, and S. M. Baylor. 1991. Myoplasmic calcium transients in intact skeletal muscle fibers monitored with the fluorescent indicator furapta. *Biophys. J. Gen. Physiol.* 97:271–301.

Konishi, M., A. Olson, S. Hollingworth, and S. M. Baylor. 1988. Myoplasmic binding of fura-2 investigated by steady-state fluorescence, and absorbance measurements. *Biophys. J.* 54:1089–1104.

Lattanzio, F. A., Jr., and D. K. Bartschat. 1991. The effect of pH on rate constants, ion selectivity, and thermodynamic properties of fluorescent calcium, and magnesium indicators. *Biochem. Biophys. Res. Commun.* 177:184–191.

Minta, A., J. P. Y. Kao, and R. Y. Tsien. 1989. Fluorescent indicators for cytosolic calcium based on rhodamine, and fluorescein chromophores. *J. Biol. Chem.* 264:8171–8178.

Monck, J. R., A. Oberhauser, T. J. Keating, and J. M. Fernandez. 1992. Thin-section ratiometric Ca^{2+} images obtained by optical sectioning of fura-2 loaded mast cells. *J. Cell Biol.* 116:745–759.

Monck, J. R., E. E. Reynolds, A. P. Thomas, and J. R. Williamson. 1988. Novel kinetics of single cell Ca^{2+} transients in stimulated hepatocytes, and A10 cells measured using fura-2, and fluorescent videomicroscopy. *J. Biol. Chem.* 263:4569–4575.

Muller, W., and J. A. Connor. 1991. Dendritic spines as individual neuronal compartments for synaptic Ca^{2+} responses. *Nature.* 354:73–76.

Neher, E. 1993. Correction for liquid junction potentials in patch clamp experiments. *Methods Enzymol.* 207:123–131.

Neher, E., and G. J. Augustine. 1992. Calcium gradients, and buffers in bovine chromaffin cells. *J. Physiol.* 450:273–301.

Nohmi, M., S. Y. Hua, and K. Kuba. 1992. Intracellular calcium dynamics in response to action potentials in bullfrog sympathetic ganglion cells. *J. Physiol.* 458:171–190.

Nowycky, M. C., and M. J. Pinter. 1993. Time courses of calcium, and calcium-bound buffers following calcium influx in a model cell. *Biophys. J.* 64:77–91.

O'Rourke, B., D. K. Reibel, and A. P. Thomas. 1990. High-speed digital imaging of cytosolic Ca^{2+}, and contraction in single cardiomyocytes. *Am. J. Physiol.* 259:H230-H242.

O'Sullivan, A. J., T. R. Cheek, R. B. Moreton, M. J. Berridge, and R. D. Burgoyne. 1989. Localization, and heterogeneity of agonist-induced changes in cytosolic calcium concentration in single bovine adrenal chromaffin cells from video imaging of fura-2. *EMBO J.* 8:401–411.

Regehr, W. G., and D. W. Tank. 1990. Optical imaging of calcium accumulation in hippocampal pyramidal cells during synaptic activation. *Nature.* 345:807–810.

Roberts, W. M. 1993. Spatial calcium buffering in saccular hair cells. *Nature.* 363:74–76.

Roberts, W. M., R. A. Jacobs, and A. J. Hudspeth. 1990. Colocalization of ion channels involved in frequency selectivity, and synaptic transmission at presynaptic active zones of hair cells. *J. Neurosci.* 10:3664–3684.

Robitaille, R., E. M. Adler, and M. P. Charlton. 1990. Strategic location of calcium channels at transmitter release sites of frog neuromuscular synapses. *Neuron.* 5:773–779.

Sala, F., and A. Hernandez-Cruz. 1990. Calcium diffusion modeling in a spherical neuron. Relevance of buffering properties. *Biophys. J.* 57: 313–324.

Segal, M., and D. Manor. 1992. Confocal microscopic imaging of $[Ca^{2+}]_i$ in cultured rat hippocampal neurons following exposure to *N*-methyl-D-aspartate. *J. Physiol.* 448:655–676.

Shroeder, T. J., J. A. Jankowski, J. Senyshyn, R. W. Holz, and R. M. Wightman. 1994. Zones of exocytotic release on bovine adrenal medullary cells in culture. *J. Biol. Chem.* In press.

Silver, R. A., A. G. Lamb, and S. R. Bolsover. 1990. Calcium hotspots caused by L-channel clustering promote morphological changes in neuronal growth cones. *Nature.* 343:751–754.

Smith, S. J., and G. J. Augustine. 1988. Calcium ions, active zones, and synaptic transmitter release. *Trends Neurosci.* 11:458–464.

Somlyo, A. V., H. Gonzales-Serratos, H. Shuman, G. McClellan, and A. P. Somlyo. 1981. Calcium release, and ionic changes in the sarcoplasmic reticulum of tetanized muscle: an electron-probe study. *J. Cell Biol.* 90: 577–594.

Takamatsu, T., and W. G. Wier. 1990. High temporal resolution videoimaging of intracellular calcium. *Cell Calcium.* 11:111–120.

Vergara, J., and M. Delay. 1986. A transmission delay, and the effect of temperature at the triadic junction of skeletal muscle. *Proc. R. Soc. Lond.* 229:97–110.

Westenbroek, R. E., M. K. Ahlijanian, and W. A. Catterall. 1990. Clustering of L-type Ca^{2+} channels at the base of major dendrites in hippocampal pyramidal neurons. *Nature.* 347:281–284.

Winegrad, S. 1970. The intracellular site of calcium activation of contraction in frog skeletal muscle. *J. Gen. Physiol.* 55:77–88.

Zhou, Z., and E. Neher. 1993. Mobile, and immobile calcium buffers in bovine adrenal chromaffin cells. *J. Physiol.* 469:245–273.